

# Vegetation Loss at D-Band Frequencies and New Vegetation-Dependent Exponential Decay Model

Brecht De Beelde, Robbe De Beelde, Emmeric Tanghe, David Plets, Kris Verheyen, Wout Joseph

**Abstract**—With the potential of fixed wireless access networks as an alternative to optical fiber, it is necessary to determine vegetation loss at millimeter wave frequencies. In this paper, we present vegetation loss measurement results for different types of vegetation, including trees, hedges, and forests, at frequencies ranging from 110 GHz to 170 GHz. An experimental method is proposed to determine the average loss per meter vegetation depth for different vegetation types. Average losses at 140 GHz range from 0.2 dB/m for an open forest, and up to 9.8 dB/m for dense hedges. As there is a large variance of vegetation loss for different vegetation types, we propose a novel vegetation-dependent exponential decay (VED) model, expressing vegetation loss as a function of vegetation depth, frequency, and vegetation density, which is expressed by the plant area index (PAI) parameter. The VED vegetation loss model can be used for network design, and to perform accurate link budget calculations.

**Index Terms**— mmWave, D-band, outdoor, channel sounding, foliage loss, vegetation, tree, hedge, modeling, fixed wireless access

## I. INTRODUCTION

Technology advancements have realized high-throughput wireless communication at millimeter wave (mmWave) frequencies, and enable applications such as fixed wireless access (FWA). These form a cheaper alternative to optical fiber links for providing high-speed internet access, as no digging is required for its deployment. In FWA networks, both antennas are typically mounted at a similar height above street level, on building facades and street furniture, forming a mesh network.

Channel models exist for the characterization of outdoor radio propagation at mmWave frequencies, and successful field trials at 60 GHz confirm that the high bandwidths provide high-throughput internet connectivity [1]–[3]. In [4], MacCartney et al. present outdoor channel measurements at 73 GHz in a dense urban environment, for a mobile user as well as a backhaul scenario with the receiving (RX) antenna at a higher height. They obtain a high correlation with channel measurements at 28 GHz, but with slightly fewer multipath components. When using directive antennas with beamsteering towards the best link, the path loss (PL) exponent of a one-slope PL model is similar to the PL exponent of sub-6 GHz models. Samimi et al. present an omnidirectional probabilistic PL model at 73 GHz, based on Line-of-Sight (LOS) and non-Line-of-Sight (NLOS) measurements, and the probability of a blockage in a dense

urban environment [5]. In [6], Zhao et al. show that a quasi-deterministic radio channel generator designed for sub-6 GHz channels can be used for simulations of fifth-generation (5G) mobile networks operational at mmWave frequency 32 GHz, based on directional measurements and channel parameter estimations via the space-alternating generalized expectation-maximization algorithm. In [7], Xing and Rappaport present outdoor channel measurements at frequencies ranging from 28 GHz to 142 GHz. They report a decreasing root-mean-squared (RMS) delay spread with increasing frequency, but the PL exponents are similar across the measured frequencies, and, therefore, outdoor wireless systems above 100 GHz will be possible. An outdoor LOS PL model at 140 GHz is presented in [8], [9].

Larger bandwidths that are available at frequencies above 100 GHz promise higher data rates for future FWA networks. Schneider et al. present link budget analyses for fixed wireless links at THz frequencies [10], and Drougas et al. present packet error rate statistics for a LOS FWA link, based on simulations [11]. Apart from generic outdoor channel models, rain attenuation and vegetation and foliage loss should be characterized in order to assess the impact on the received power in a wireless system. Shamsan models rainfall for mmWave FWA systems [12]. Multiple models exist for the characterization of vegetation loss at sub-6 GHz frequencies. Current mmWave vegetation loss models are based on measurements below 60 GHz and are applicable for frequencies up to 100 GHz.

In this paper, we present vegetation loss measurements at D-band frequencies, ranging from 110 GHz to 170 GHz, and a novel model is provided for calculating vegetation loss as a function of frequency and vegetation characteristics. The outline of this paper is as follows. In Section II, we first provide a background on existing vegetation loss models, as well as on vegetation characterization. In Section III, we present the channel sounder and measurement scenarios. The measurement results are presented in Section IV, and a vegetation-dependent exponential decay (VED) model is presented in Section V. Section VI concludes this paper.

## II. BACKGROUND

### A. Vegetation loss models and measurement campaigns

Multiple exponential decay models exist to model the attenuation due to vegetation and foliage obstructing the propagation path. These models have the generic form of

$$L(f, d)[\text{dB}] = A f^B d^C, \quad (1)$$

with  $f$  the frequency in MHz or GHz and  $d$  the vegetation depth in meters. Model parameters  $A$ ,  $B$ , and  $C$  are estimated

B. De Beelde, E. Tanghe, D. Plets and W. Joseph are with Ghent University/IMEC, Department of Information Technology, Ghent, Belgium. R. De Beelde and K. Verheyen are with Ghent University, Department of Environment, Ghent, Belgium. E-mail: Brecht.DeBeelde@UGent.be

from measurement data. Table I lists the fitted parameters for different well-known models. The Weissberger model [13] is based on measurements for dry and dense foliage, with frequencies up to 95 GHz. The recommendation by the international radio consultative committee (CCIR) uses a similar model, with adjusted parameters [14]. When both antennas are far enough from the trees, diffraction over the foliage is found to be the main propagation mechanism [15]. The COST235 model distinguishes between two scenarios: deciduous trees having leaves (in summer) and not having leaves (in winter) [16]. Measurements performed by Al-Nuaimi and Stephens in a pine woodland resulted in an updated FITU-R model with a recommended model for use with frequencies up to 40 GHz [17]. The model takes into account vegetation type, vegetation depth, and the illuminated area of the foliage. The recommendation also provides diffraction loss and ground reflection models.

Next to the exponential decay models, other models exist. One example is the following maximum attenuation model:

$$L(f, d)[\text{dB}] = A_{\max} \left( 1 - e^{-\frac{d\gamma}{A_{\max}}} \right), \quad (2)$$

with  $A_{\max} = Af^B$  the maximum attenuation, and  $\gamma$  the specific attenuation in dB/m [18]. Parameters  $A$ ,  $B$ , and  $\gamma$  are empirically determined and depend on the vegetation type. Fitting vegetation loss of tropical woodland for frequencies below 2 GHz to this model results in  $A = 0.18$ ,  $B = 0.752$ , and  $\gamma = 0.0063 f^{0.537}$  [19]. For a single vegetative obstruction, i.e., both antennas are outside the vegetation area, and frequencies below 3 GHz, the vegetation loss can be simplified to  $L = d\gamma$ , with  $d$  the vegetation depth and  $\gamma$  the specific attenuation in dB/m. For frequencies above 5 GHz, the following non-zero gradient model can be used:

$$L(d)[\text{dB}] = \gamma_{\infty}d + k \left( 1 - e^{-\frac{(\gamma_0 - \gamma_{\infty})d}{k}} \right), \quad (3)$$

with  $\gamma_0$  the initial specific attenuation in dB/m,  $\gamma_{\infty}$  the final specific attenuation in dB/m, and  $k$  the final attenuation offset in dB [20]. The dual gradient model, even though it is found to be inaccurate [17], is the only model that takes into account the antenna beamwidth [21], [22].

The COST235 and FITU-R model provide fitted parameters that depend on the leaf state. The seasonal differences for tundra vegetation are studied by Romanov and Ulanov [23]. Schwering et al. investigate mmWave propagation in summer and winter conditions and apply the theory of radiative energy transfer (RET) to model mmWave propagation in woods and forests [24]. The RET model defines attenuation due to scattering through vegetation with vegetation depth, beamwidth and absorption and scattering coefficients as input parameters. Horak et al. study the frequency dependence of vegetation loss at sub-6 GHz frequencies [25] for satellite services, i.e., using different elevation angles, and report average losses ranging from 9 dB at 2 GHz to 14.5 dB at 6 GHz. An empirical propagation model at 900 MHz and 2.4 GHz for a forest environment at tree trunk level, i.e., with limited foliage, is presented by Azevedo et al. [26]. Sub-GHz measurements in a forest terrain for distances up to 2.5 km show that the above models tend to over-estimate vegetation loss at large distances

[27]. Near-ground propagation in presence of vegetation is also simulated by Liao and Sarabandi [28], and by DaHan and Sarabandi [29].

Several studies have been presented on the impact of vegetation on radio propagation at mmWave frequencies up to 100 GHz [24], [30]–[35]. Perras and Bouchard discuss fading characteristics due to foliage, for frequencies up to 60 GHz [30]. Zhang et al. present a site-specific model at 28 GHz for forest environments [31], using the foliage area and fitting specific attenuation for different area boundaries. Lv et al. create an exponential model based on measurements at 39 GHz [32]. Zhang et al. characterize a vegetated suburban environment at 28 GHz and 39 GHz for 5G mmWave communication [33], reporting that vegetation results in a high delay and angular spread. Ko et al. study radio propagation at 28 GHz for a vegetated residential environment [34] via directional measurements. They compare attenuation of the best path to attenuation when summing all angular powers, and show that the exponential model from (1) results in a lower root-mean-squared error (RMSE) than the model from (2). Wideband measurements at 61.5 GHz are presented by Rogers et al. in [35]. Directional measurements at 20 GHz and 62.4 GHz are used in [36] to evaluate the performance of a discrete RET-based modeling approach in which the vegetation medium is discretized into cells for which the signal is decomposed into coherent and diffuse components. Ray-tracing based models for mmWave propagation through vegetation are presented in [37], [38] and use measurements to derive scattering profiles from trees.

## B. Forest characterization

Different metrics are used for the characterization of vegetation. A first characterization is the tree species composition and the average trunk diameter of the different species, which is reported as the average tree diameter at breast height (ADBH). Fractional vegetation cover (FVC), leaf area index (LAI), and plant area index (PAI) are metrics that indicate how dense the vegetation is. FVC is defined as the ratio of the vertical projection area of vegetation (including leaves, stalks, and branches) on the ground to the total vegetation area, and is an important parameter used to measure surface vegetation cover [40]. We transform the concept of FVC from the vertical plane to the horizontal plane. Horizontal FVC (HFVC) is defined as the fraction of area that is covered by vegetation between two antennas. An HFVC of 0% corresponds to free space, whereas an HFVC of 100% means that the first Fresnel zone of the link is at one point completely blocked by vegetation.

Plant canopy and foliage density are characterized by the LAI, which is a dimensionless quantity defined as the green leaf area per unit ground surface area and therefore, depends on the leaf state. An LAI of 5 means that the single-sided surface of all leaves that are present above an area of 10 m<sup>2</sup> equals 50 m<sup>2</sup>. LAI is related to FVC and the Beer-Lambert law, which expresses an exponential relation between light intensity and absorbance, and can be used to estimate LAI [41], [42].

Table I  
EXISTING EXPONENTIAL DECAY FOLIAGE MODELS.

Name	A	B	C	Frequency unit	Frequency range	Applicability	Reference
Weissberger	1.33	0.284	0.588	GHz	0.23 - 95 GHz	$d \in [14, 400]$ m	[13]
Weissberger	0.45	0.284	1	GHz	0.23 - 95 GHz	$d \in [0, 14]$ m	[13]
CCIR	0.2	0.3	0.6	MHz	0.2 - 95 GHz	$d \in [0, 400]$ m	[14]
COST235	15.6	-0.009	0.26	MHz	9.6 - 57.6 GHz	$d \in [0, 200]$ m	[16]
FITU-R	0.39	0.39	0.25	MHz	9 - 40 GHz	$d \in [0, 200]$ m	[17]
Horak et al.	1.43	0.884	0.043	GHz	2 - 6 GHz	single tree crown	[39]
Lv et al.	2.143	0.078	0.650	MHz	38 - 40 GHz	$d \in [2.9, 11.8]$ m	[32]
Ko et al.	0.805	0.261	0.277	MHz	28 GHz	$d \in [20, 370]$ m	[34]

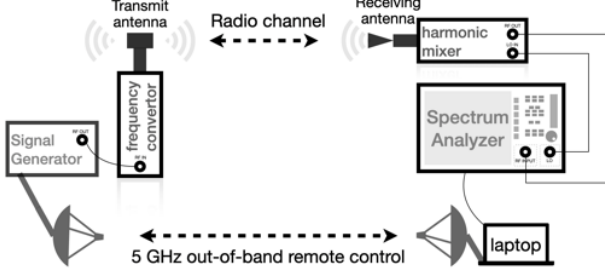


Figure 1. Channel sounder architecture.

As propagation through vegetation is not only influenced by the amount of leaves present, but also by trunks and branches, it is more appropriate to consider PAI as a parameter influencing the vegetation loss. PAI is defined as the area of all leaves and branches per unit surface area, and depends on the tree composition and age of the forest. As an example, the PAI is expected to increase with height for an older forest, as the foliage at crown level is denser. A younger forest has a higher PAI, even for lower heights. Also, the PAI near forest edges is typically higher than in forest interiors. Nominal values of LAI/PAI for the different vegetation types we considered can be found in literature [43]–[47].

### III. METHODOLOGY

#### A. Channel sounder design

We use a spectrum analyzer-based channel sounding approach. The channel sounding setup is presented in Fig. 1. A signal generator generates a radio frequency source in frequency range 9.1 to 14.1 GHz that is up-converted to the D-band using a frequency multiplier. A vertically polarized omnidirectional transmitting (TX) antenna with a gain of 3 dBi is connected to the frequency multiplier's rectangular waveguide (WR-6). At the receiving side, a directional RX horn antenna is connected to a harmonic mixer that down-converts the received signal at D-band frequencies to an intermediate frequency (IF) signal from which the amplitude is analyzed by a spectrum analyzer. The RX antenna has an azimuth half-power beamwidth (HPBW) of  $12^\circ$ , an elevation HPBW of  $9.5^\circ$ , and a gain of 23 dBi. A point-to-point wireless link at 5 GHz is used for remote control of the signal generator.

Using a resolution bandwidth of 100 Hz, the displayed average noise level of the spectrum analyzer is -151 dBm. The noise figure of the spectrum analyzer's IF port is 3 dB, and the

conversion loss of the mixer is 30 dB. We performed measurements for frequencies ranging from 110 GHz to 170 GHz, in steps of 1 GHz. With a transmit power of 8 dBm at the antenna input, we can measure PL up to 140 dB.

From the received power, we calculate PL via

$$PL = P_{TX} - P_{RX} + G_{TX} + G_{RX} + C, \quad (4)$$

with  $P_{TX}$  the transmit power in dBm,  $P_{RX}$  the measured received power in dBm which takes into account the conversion loss of the mixer,  $G_{TX}$  and  $G_{RX}$  the antenna gain of the TX and RX antennas in dBi, and  $C$  a frequency-dependent correction factor in dB based on calibration data. The loss of the cable connecting the frequency multiplier to the signal generator is corrected for on the signal generator. Both antennas are leveled horizontally and placed at the same height, by using a 3-point leveled rotational platform. Height and distance adjustments are made using a laser positioning system. We perform angular measurements by rotating the RX antenna in steps of  $12^\circ$  and investigate the angular PL profile. From the angular PL profile, we calculate PL as a function of RX antenna beamwidth via

$$PL = P_{TX} + G_{TX} + G_{RX} - 10 \log_{10} \left( \sum_{\theta \in \Theta} P_{RX}(\theta) \right), \quad (5)$$

with  $P_{TX}$  the transmit power,  $G_{TX}$  and  $G_{RX}$  the antenna gains, and  $P_{RX}(\theta)$  the received power for RX azimuth angle  $\theta$ , calculated via  $P_{RX}(\theta) = 10^{(P_{TX} + G_{TX} + G_{RX} - PL(\theta))/10}$  with  $PL(\theta)$  the corrected PL that is calculated via (4). We sum the received powers for  $\theta$  in  $\Theta$ , which is the set of azimuth angles that encompass the beamwidth. At 140 GHz, we can sum linear received powers, as the angular step size equals the HPBW of the RX antenna. We calculate angular spread (AS) in degrees via

$$AS = \frac{180}{\pi} \sqrt{-2 \ln \left( \left| \frac{\sum_{\theta \in \Theta} e^{j\theta} P_{RX}(\theta)}{\sum_{\theta \in \Theta} P_{RX}(\theta)} \right| \right)}, \quad (6)$$

with  $P_{RX}(\theta)$  the linear received power at 140 GHz for azimuth angle  $\theta$  in radians [48]. For the AS calculation, the azimuthal range  $\Theta \in [-60^\circ, 60^\circ]$  is considered for all environments.

We define vegetation loss as the excess loss equal to the difference between measured PL, obtained via (4), and the free space PL (FSPL) corresponding to the path distance between the TX and RX antennas. We get normalized vegetation loss per meter by dividing the vegetation loss by the vegetation depth. To compare the loss of different vegetation types, we average over the different vegetation depths to obtain an averaged normalized vegetation loss.

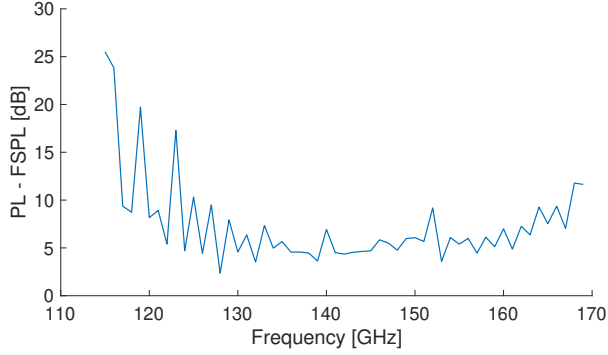


Figure 2. Median of the error between measured Line-of-Sight and free space path loss as a function of frequency, across the reference distances ranging from 2 m to 10 m.

### B. Calibration

We performed reference measurements in an outdoor unobstructed environment, for distances ranging from 2 m to 10 m and with the directional RX antenna pointing towards the TX antenna, to obtain the correction factor  $C$  in (4). Both antennas are leveled horizontally. Figure 2 shows the median error between measured PL and FSPL as a function of frequency. The frequency-dependent variation of the error is caused by the gain variation of 2 dB of the omnidirectional antenna over its frequency range, and by the cable losses of the cables connecting the harmonic mixer to the spectrum analyzer, as these cable losses are not taken into account when converting measured received power to PL. The larger error for frequencies below 120 GHz is caused by a poor antenna performance for these frequencies and is confirmed by  $S_{11}$  and  $S_{21}$  test data provided by the antenna's manufacturer. The harmonic mixer's conversion loss is also frequency-dependent, but the calibration data provided by the mixer's manufacturer is taken into account in the conversion.

The offset between the LOS PL measurements and FSPL does not depend on the distance between the antennas, with a mean standard deviation of 0.75 dB and a maximum standard deviation of 1.33 dB across the different distances for frequencies from 120 to 160 GHz. Therefore, for all frequencies, we take the median value of the error between measured PL and FSPL of all distances and use this as the correction factor  $C$  when determining PL via (4).

### C. Measurement environments and scenarios

We performed vegetation loss measurements in 12 different measurement environments for the different types of vegetation and cultivation listed in Table II. For each vegetation type, we define HFVC, PAI, and tree species composition. The location of the first 4 measurement environments is at a university campus, i.e., a suburban environment. Measurement environments 1 and 3 have the same vegetation in between and are representative of a tree crown. Environments 5 and 8 are located in a young forest, characterized by trees with a small diameter, low shrubs, and a dense forest edge. The RX antenna moves parallel with the edge. Environments 6, 7, and



(a) Picture of the measurement setup with an antenna separation of 8.7 m

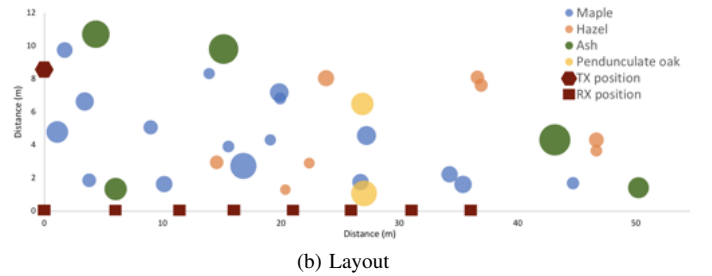


Figure 3. Measurement environment 6.

9 to 12 are located in another forest [49], [50]. Environments 6 and 7 are in the younger part of the forest, again with smaller tree diameter and more twigs, whereas, environments 11 and 12 are in the older part of the forest, with more tree trunks, and fewer foliage and twigs. For each measurement environment and vegetation depth, we took a picture of the vegetation which is used as input for the Gap Light Analyzer tool [51] that determines PAI based on pictures. This PAI value is combined with the tree layout plan and a human estimate into a PAI estimate for every measurement. Table II also contains this PAI estimate, as well as an HFVC estimate. The azimuthal scanning range depends on the environment. For the forest, we want to capture all multipath components and scan the full  $360^\circ$ , whereas we only scan from  $-60^\circ$  to  $60^\circ$  for the single trees and hedges, in order to not capture environmental reflections that are not related to the vegetation. As an illustration, Fig. 3 shows a picture and the tree layout of environment 6. An overview of all measurement environments and scenarios is provided in the Appendix.

Based on the measurement setup, we define vegetation depth as the distance over which the vegetation obstructs the LOS path. For environments 1 to 4, this differs from the obstructed LOS path distance as the antennas are outside the vegetation area, whereas for locations 5 to 12, the vegetation depth equals the path distance. For each measurement environment, we perform measurements with different vegetation depths, by moving the antennas.

The measurements are performed in the horizontal plane, i.e., both antennas are at the same height, as this is rep-

Table II  
DESCRIPTION OF THE DIFFERENT MEASUREMENT ENVIRONMENTS, WITH HFVC THE HORIZONTAL FRACTIONAL VEGETATION COVER, PAI THE PLANT AREA INDEX AND ADBH THE AVERAGE TREE DIAMETER AT BREAST HEIGHT (1.3 M) IN CM

Environment ID	Category	Composition	HFVC	PAI	ADBH	Vegetation depth	Azimuthal scan
1	tree	<i>R. pseudoacacia</i> L. (Black locust)	90%	5	15 cm	11.4 to 16.2 m	-60° to 60°
2	single hedge	<i>P. laurocerasus</i> L. (Common laurel)	100%	9		4 m	-60° to 60°
3	tree	<i>R. pseudoacacia</i> L. (Black locust, 80%), <i>Fraxinus exelsior</i> L. (Ash, 20%)	95%	6	25 cm	0 to 7.5 m	-60° to 60°
4	tree	<i>C. avellana</i> L. (Hazel)	95%	5	35 cm	0 to 9.4 m	-60° to 60°
5	hedge	<i>Q. rubra</i> L. (Red oak, 70%), <i>C. avellana</i> L. (Hazel, 20%), <i>F. sylvatica</i> L. (Beech, 5%), <i>Crataegus monogyna</i> J. (Hawthorn, 5%)	70%	4	20-45 cm	10.5 to 20.8 m	-84° to 84°
6	deciduous forest	<i>A. pseudoplatanus</i> L. (Maple, 55%), <i>C. avellana</i> L. (Hazel, 25%), <i>Fraxinus exelsior</i> L. (Ash, 15%), <i>Q. Robur</i> L. (Pedunculate oak, 5%)	65%	2	30 - 45 cm	8.7 to 37.2 m	-180° to 180°
7	deciduous forest	<i>C. avellana</i> L. (Hazel, 60%), <i>A. pseudoplatanus</i> L. (Maple, 30%), <i>Fraxinus exelsior</i> L. (Ash, 10%)	55%	1	30 - 45 cm	10.5 to 34.0 m	-180° to 180°
8	dense hedge	<i>Q. rubra</i> L. (Red oak, 65%), <i>C. avellana</i> L. (Hazel, 35%)	100%	3	20 - 30 cm	4.75 to 6.5 m	-72° to 72°
9	tree trunk	<i>Q. robur</i> L. (Pedunculate oak)					
10	forest	<i>C. avellana</i> L. (Hazel, 70%), <i>Q. robur</i> L. (Pedunculate oak, 30%)	20%	0.8	55 cm	7.1 to 16 m	-72° to 72°
11	open forest	<i>C. avellana</i> L. (Hazel, 80%), <i>Q. robur</i> L. (Pedunculate oak, 20%)	10%	0.4	55 cm	15 to 20.8 m	-72° to 72°
12	open forest	<i>F. sylvatica</i> L. (Beech, 70%), <i>A. pseudo-platanus</i> L. (Maple, 20%), <i>L. decidua</i> M. (Larch, 10%)	2%	0.2	65 cm	40 to 48 m	-48° to 48°

representative for FWA applications, where the antennas are at a similar height. Furthermore, this results in a more precise measurement setup. As we use a highly directive RX antenna, a slight deviation in tilt would result in a significant decrease of received power and an overestimation of vegetation loss.

#### D. Validation

The harmonic mixer has a frequency-dependent conversion loss that is taken into account in the spectrum analyzer, based on calibration test data provided by the manufacturer. The cable loss of the cable connecting the frequency multiplier to the signal generator is measured and corrected on the signal generator. The attenuation of the cables connecting the mixer's IF and LO ports is not taken into account and the TX antenna has gain variations up to 2 dB in the considered frequency band. The antenna and cable variations are fixed and taken into account via the reference measurements, outlined in Section III-B. Measurements with the same measurement setup are presented in [52] and show that the received power level also depends on atmospheric conditions, as the equipment is sensitive to temperature variations. PL variations up to 1 dB are measured.

In order to validate the measured PL, we have performed unobstructed LOS measurements at the vegetation locations. For measurements without any vegetation obstruction, we add the offset to the measured PL and compare it to free space PL. The mean difference between the measured PL for an unobstructed path, and FSPL, is 0.7 dB for frequency 140 GHz. The difference is larger for the measurement locations in the forest, compared to the measurements performed at the university campus, but it is smaller than 3 dB for all measurement locations.

## IV. MEASUREMENT RESULTS

### A. Angular PL

Figure 4 presents the angular PL for environments 3, 6, and 10. For most of the measurement scenarios, the minimum PL corresponds to the obstructed direct path, i.e., with the RX antenna directed towards the TX antenna. However, for scenarios where a tree trunk is obstructing the direct path, a reflected path with an angle of arrival (AoA) different from 0° has a lower PL. This is the case for the measurement with a vegetation depth of 7.5 m at environment 3. At environments 6 and 7, a full 360° azimuthal scan is performed, and strong back reflections are observed, i.e., with an AoA around 180°, which is in line with the observations of backscattering at mmWave frequencies in [36]. The measurements with an absolute AoA below 54° have a measured PL well below the maximum measurable PL of the channel sounder. From the angular PL, we conclude that multipath components with different AoAs contain similar amounts of power. Therefore, vegetation loss based on omnidirectional PL would be considerably lower.

Averaged AS values for an azimuthal scanning range of -60° to 60° at frequency 140 GHz are reported in Table III. For environments 3, 4, 5, 6, and 10, the AS ranges from 13° to 15°, which is in line with the values for vertically co-polarized measurements reported in [32]. For environments 11 and 12, the average AS is 5.9° and 7.9°, respectively. The AS can be intuitively explained by diffuse scattering. The tree trunks absorb most of the electromagnetic power, but it is expected that scattering by the leaves and branches, with dimensions in the order of wavelengths, causes the lower received power and contributes to the vegetation loss. The lower PAI of environments 11 and 12 results in less scattering,



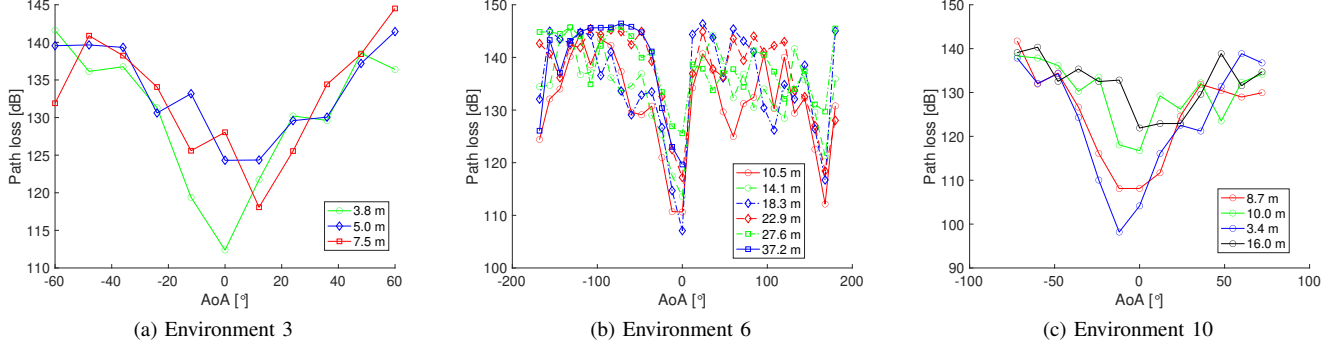


Figure 4. Measured path loss at 140 GHz as a function of AoA for different vegetation depths.

Table III  
ANGULAR SPREAD (AS) AT 140 GHz AND NORMALIZED VEGETATION LOSS IN DB PER METER VEGETATION DEPTH FOR D-BAND FREQUENCIES FOR DIFFERENT VEGETATION MEASUREMENTS.

ID	AS	120 GHz	125 GHz	130 GHz	135 GHz	140 GHz	145 GHz	150 GHz	155 GHz	160 GHz
1	18.2°	1.63	1.60	1.66	1.83	1.66	1.72	1.69	1.40	1.30
2	25.1°	10.67	10.20	10.73	9.78	9.49	9.24	10.08	9.79	9.47
3	14.7°	4.19	3.49	3.95	4.55	3.87	4.41	4.01	3.46	3.78
4	15.4°	2.16	2.03	2.04	2.00	1.95	2.11	2.22	1.75	1.54
5	13.1°	0.86	0.94	1.13	1.13	1.17	1.04	0.91	0.94	0.93
6	12.6°	0.24	0.46	0.38	0.35	0.35	0.25	0.25	0.19	0.22
7	10.5°	-0.01	0.01	0.07	0.12	0.01	0.04	-0.03	0.04	-0.00
8	11.7°	0.85	1.31	2.16	2.31	2.18	1.69	1.78	1.66	1.43
10	13.2°	0.66	0.80	0.64	0.83	0.82	0.72	0.79	0.61	0.62
11	5.9°	0.10	0.01	0.03	0.04	0.03	0.09	0.16	0.11	0.17
12	7.9°	0.23	0.25	0.24	0.28	0.20	0.22	0.21	0.19	0.22

and therefore, lower received power for AoAs different from  $0^\circ$ .

### B. Vegetation loss obstructed direct path

Figure 5 shows the vegetation loss as a function of frequency for measurements with different vegetation depths in environment 6. At lower frequencies, vegetation loss increases with increasing frequency, which is illustrated by the frequency dependence of the specific attenuation reported in [18] and the positive frequency exponent in the Weissberger [13], CCIR [14] and FITU-R [17] models. From our measurements, and illustrated in Fig. 5, we conclude that vegetation loss at D-band frequencies decreases with increasing frequency. This can be explained by the smaller Fresnel radius at higher frequencies, allowing radio propagation via the gaps in the foliage structure and tree canopy. Similar conclusions are drawn at mmWave frequencies, and result in the negative frequency exponent reported in [16].

Vegetation loss is not linearly dependent on vegetation depth, which is clear from the parameter C in (1) that differs from 1 for all models except the Weissberger model for small distances. However, to analyze the frequency and vegetation dependence, averaged normalized vegetation loss values of the direct path are presented in Table III in dB/m. These values do not provide an accurate model, but they allow comparing vegetation loss for different environments, as similar vegetation depths are considered for most environments.

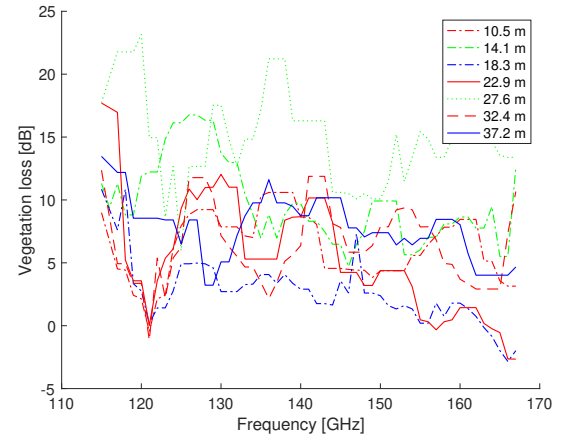


Figure 5. Vegetation loss for different vegetation depths for AoA  $0^\circ$  as a function of frequency for vegetation environment 6.

A tree with large vertical coverage (i.e., environment 1) causes significant attenuation, ranging from 1.3 dB/m to 1.8 dB/m. A dense hedge results in an even higher attenuation of up to 10 dB/m. For the trees from environment 3, attenuation up to 4.5 dB/m is larger than for environment 1 and environment 4, which can be explained by the larger diameter of the trees, resulting in more blockage. For environment 4, the coverage is 100% but consists of leaves (and fewer branches), resulting in attenuation values around 2 dB/m. For

environment 5, the attenuation is even lower, i.e., around 1 dB/m, which is caused by the vegetational structure. There is a hedge near the RX antenna positioned near the border edge, but in between the hedge and the TX antenna, there is lower vegetation that does not block the signal.

Even though environments 6 and 7 have the same type, i.e., the same forest but at a slightly different location, the average vegetation loss for environment 7 is lower. In line with the lower coverage, vegetation loss is much lower than for environments 1 to 5. Environment 8 is located near environment 5, and measures vegetation loss due to a dense edge, with values up to 3 dB/m. It should be noted that for distance 4.75 m, there was an opening in the hedge, resulting in zero attenuation. For environment 10, a similar vegetation loss as environments 5 and 6 is found, which is in line with the vegetation coverage. Environments 11 and 12 are in an open forest, where there is no foliage and a free space environment can be considered.

Compared to an extrapolation of the Weissberger, CCIR and COST235 models to D-band frequencies, the measured vegetation loss is lower. For distances ranging from 10 m to 20 m, the Weissberger model predicts a vegetation loss ranging from 21 dB to 32 dB, the CCIR model predicts an vegetation loss from 28 dB to 42 dB, and the COST235 model predicts a vegetation loss ranging from 25 dB to 30 dB. The measured vegetation loss is also lower than the FITU-R model and lower than the reported value of 20.8 dB for distances around 10 m, reported in [32]. Due to the small wavelength corresponding to D-band frequencies, the vegetation cannot be considered a homogeneous medium and a lower vegetation loss is observed.

### C. Antenna beamwidth dependence on vegetation loss

From the angular PL profiles, we conclude that the contribution of reflected power is significant. Therefore, the beamwidth of the antenna used in the system will influence the amount of received power. We derive vegetation loss as a function of antenna beamwidth by summing linear received powers of multiple RX antenna orientations. Figure 6 presents vegetation loss at 140 GHz as a function of antenna beamwidth. The loss decreases significantly when extending the beamwidth from 12° to 36°, i.e., combining the received power from 3 RX antenna orientations.

Using RET theory, propagation in vegetative environments can be modeled by means of coherent and incoherent components [24]. Attenuation of the coherent components, with a well-defined propagation direction and propagation, is caused by absorption and reflection, whereas incoherent components are introduced by scattering and have random propagation directions and polarizations [53]. An antenna with a larger beamwidth receives more incoherent components, which results in a lower vegetation loss as reported in [36]. For larger beamwidths, the loss further decreases, but more slowly. Comparing the vegetation loss as a function of antenna beamwidth for different vegetation depths, we do not observe a relation between the beamwidth dependence and vegetation depths. Therefore, we conclude that the incoherent components are

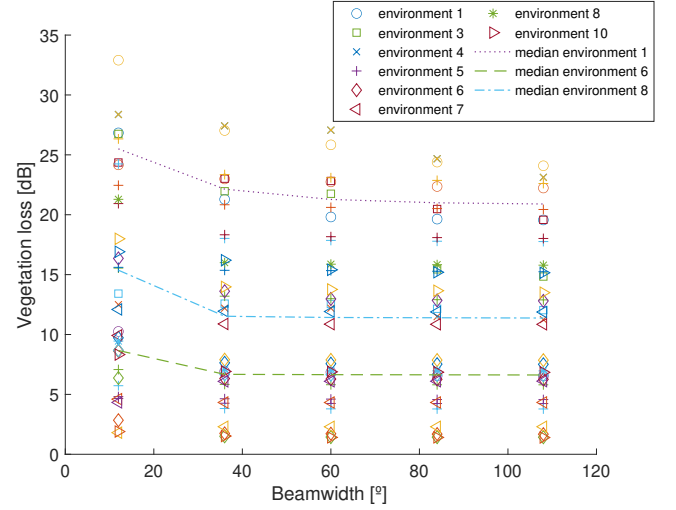


Figure 6. Measured vegetation loss at 140 GHz as a function of antenna beamwidth.

dominant. This can be explained by the leaf dimensions that are similar to the wavelength and cause a large degree of scattering, but also by the smaller Fresnel radius that allows more radio propagation via gaps in the vegetation. Furthermore, absorption loss increases with frequency [8], which causes the coherent components to be more attenuated.

### D. Tree trunk

We also measured signal attenuation when a single tree obstructs the direct path, in measurement environments 3 and 9. Compared to the scattering effect of leaves, signal attenuation due to a tree trunk obstruction is caused by absorption. For environment 3, with diffraction around a black locust tree with a diameter of 0.3 m and a total distance of 8.4 m between the antennas, the signal attenuation ranges from 15 dB to 23 dB, which is higher than the attenuation ranging from 5 dB to 15 dB due to tree trunks at sub-6 GHz frequencies [26]. For environment 9, the attenuation due to diffraction around a pedunculate oak with a diameter of 0.6 m and a distance of 6.3 m between the antennas, increases to 30 dB. In this case, a lower attenuation of 27 dB is obtained when the RX antenna is rotated by 12°, due to a lower diffraction angle causing a lower diffraction loss.

## V. VEGETATION-DEPENDENT EXPONENTIAL DECAY (VED) MODEL

From the measurement results presented in the previous section, we conclude that there are large differences in vegetation loss, depending on the vegetation type. The vegetation loss slightly decreases with frequency, but there is no strong dependence on frequency, as the wavelengths over the full band compared to the size of the environmental objects (i.e., leaves, branches, tree trunks) are similar. Indeed, the wavelength at 110 GHz is 2.7 mm, whereas it is 1.8 mm for 170 GHz, and both are much smaller than the typical object dimensions.

### A. Current exponential decay models

When fitting the measurement data to the exponential model from (1), the frequency exponent  $B$  is negative, i.e., vegetation loss decreases with increasing frequency, which corresponds to the observation of Fig. 5. This is similar to the COST235 model. Parameter  $A$  is 2.6 for environment 1, 5.5 for environment 5, and increases up to 52.3 for environment 4. For the latter, the distance exponent  $C$  is smaller, i.e., 0.9 compared to 1.5 for environment 1. As expected, there are large variations between the different environments and the fitted model has a low coefficient of determination of 0.20. If we extrapolate the CCIR, FITU-R and COST235 model parameters to D-band frequencies, all models over-estimate vegetation loss at 140 GHz, with an RMSE of 19 dB between the extrapolated COST235 model and our measurement data, and up to 30 dB for the CCIR, FITU-R and Weissberger models. The large RMSE values are partly caused by the low vegetation losses measured in the forest environments 6, 7, and 12. If we compare the measured data for distances below 20 m, the RMSE between the measurement data and the COST235 model is 16 dB. The RMSE is 20 dB for the CCIR model, 25 dB for the FITU-R model, and 15 dB for the Weissberger model.

### B. Novel VED model

Based on the measurement results presented in Table III, we propose the following vegetation-dependent exponential decay (VED) model

$$L(p, d, f)[\text{dB}] = Af^B d^C p^D, \quad (7)$$

which expresses vegetation loss in dB as a function of PAI  $p$ , vegetation depth  $d$  in meter, and frequency  $f$  in GHz for frequencies in the D-band.

Fitting measured vegetation loss to this model results in  $A = 20.4$ ,  $B = -0.4$ ,  $C = 0.3$ , and  $D = 0.9$ . The RMSE between the measured PL data and fitted model is 5.6 dB, which is smaller than the RMSE values reported in [31], [32], and the coefficient of determination increases from 0.20 for the exponential decay model to 0.67 when considering PAI. The regression parameter  $D$  was found to be significant at the 5% level, with a  $p$ -value below  $10^{-3}$ . The amount of absorbing and scattering matter is also related to the distance between the antennas, as a larger distance implies more vegetation. When analyzing the differences between the measured PL and VED model, differences exceeding 3 dB are found when there is a tree with a large diameter blocking the LOS path near the receiver.

In our model, PAI is used to characterize the density of a non-homogeneous medium. If we use the HFVC as the metric, the RMSE increases to 8 dB, and the coefficient of determination decreases to 0.34.

### C. Model usage

By using PAI as the model parameter, it is also possible to extrapolate the measurement results and VED model to other vegetation types, using PAI values for different vegetation

types that are available in literature [54]–[56]. As the PAI depends on the canopy height [57], [58], the VED model can be used to estimate vegetation loss for different antenna heights, by using the PAI corresponding to the foliage at the given height. This is illustrated by the following example. If both antennas are mounted at a height of 25 m in the forest of environment 6, they are at the crown level of the maple trees and the expected PAI is 5 [56], which is higher than the PAI of 2 for an antenna height of 1.3 m. For a vegetation depth of 10 m, the vegetation loss at 145 GHz increases from 10.4 dB to 23.7 dB for the higher antenna height.

If only the LAI is known, i.e., the one-sided surface of all leaves, and not the PAI, which includes the tree stem and branches, the typical woody-to-total-plant-area ratio can be used to calculate the PAI based on LAI [43]. Furthermore, satellite-based LAI estimates are available for different geographic regions [59]. This allows using the VED model using a PAI estimate based on the geographic location if the exact forest composition is not known.

## VI. CONCLUSIONS

In this paper, the results and analysis of vegetation loss measurements at D-band frequencies are presented to characterize signal attenuation in a vegetated environment for FWA applications. Compared to sub-6 GHz and lower mmWave frequency bands, there is no increase of vegetation loss with increasing frequency, and existing vegetation models overestimate vegetation loss after an extrapolation to D-band frequencies. Azimuthal angular spread values range from  $15^\circ$  to  $25^\circ$ , and with an antenna beamwidth of  $36^\circ$ , a lower vegetation loss is obtained as scattered power is received. As the vegetation density has a significant influence on the vegetation loss, we propose a new model to predict vegetation loss as a function of frequency, distance, and vegetation type. The density of the vegetation is characterized by the plant area index (PAI). Using this PAI, the model allows estimation of vegetation loss for different types of vegetation, but also for different antenna heights, by using the appropriate PAI for the corresponding tree height.

## ACKNOWLEDGMENT

This work was executed within the imec D-band channel modeling research project (D-BARC) and COST Action CA20120 (INTERACT). The authors would like to thank the reviewers and editors for their valuable feedback.

## APPENDIX

A schematic overview of all measurements at the different environments is presented in Fig. 7. For each measurement, the path distance (PD) and vegetation depth (VD) are provided. Validation measurements are represented by dashed blue lines between the TX and RX. Figure 8 provides a picture of the different measurement environments. The location where the pictures from Fig. 8 are taken is indicated in Fig. 7 with a camera symbol.



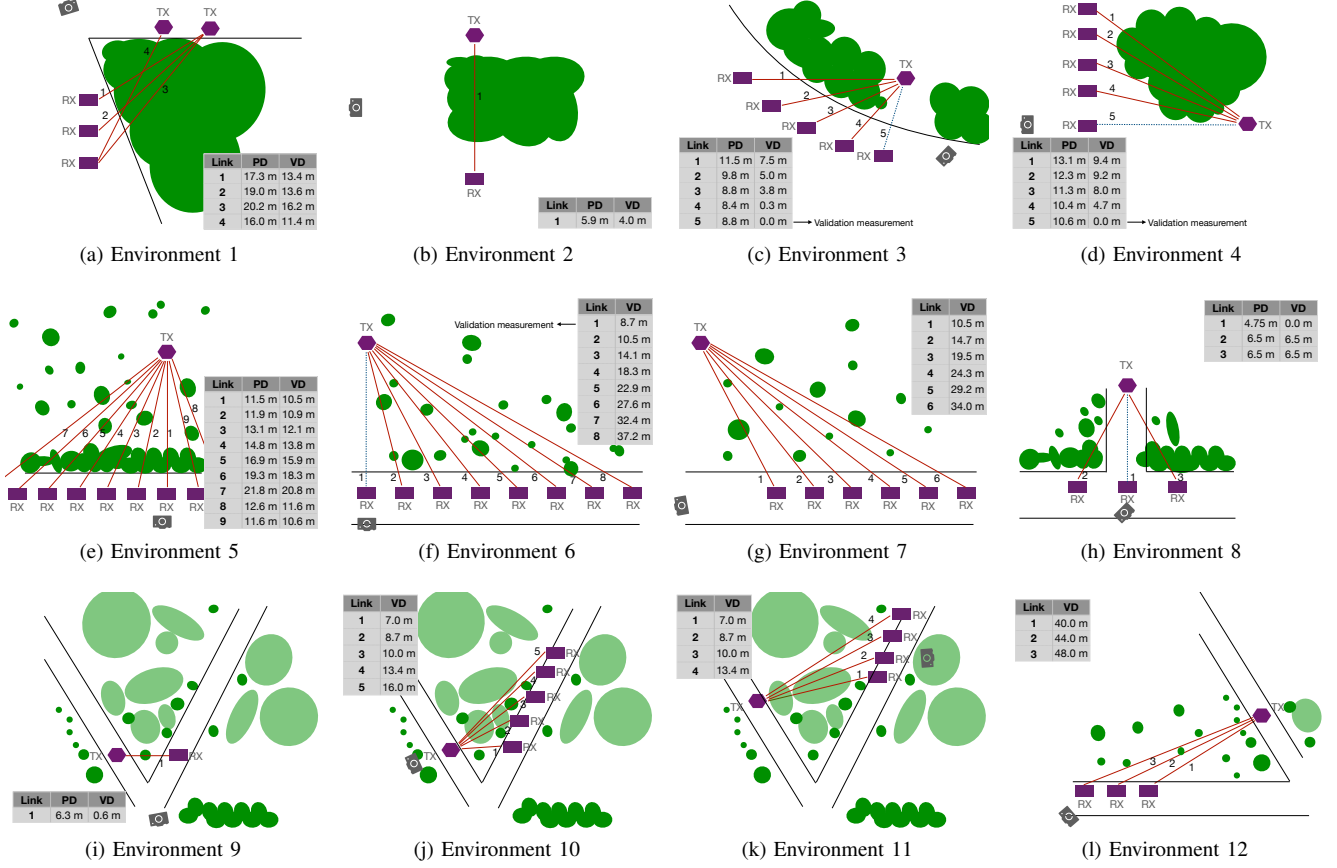


Figure 7. Measurement scenarios for different measurement environments. TX antenna locations are represented by hexagons, RX antenna locations by rectangles. For each measurement, represented by a red line, the path distance (PD), i.e., antenna separation, and vegetation depth (VD) are listed. LOS validation measurements are represented by dashed blue lines. The camera symbol indicates where the pictures shown in Fig. 8 are taken from.

## REFERENCES

- [1] K. Henke, A. Balogh, and J. Benz, "Path to commercialization: From technical trial to commercial pilot," Telecom Infra Project, Tech. Rep., 2020.
- [2] M. Glover, "TeraGo advances 5g fixed wireless technical trials," TeraGo, Tech. Rep., 2021.
- [3] W. van Thillo, "Pharrowtech, telenet, and unitron secure public funding for fixed wireless access field trial," TeraGo, Tech. Rep., 2021.
- [4] G. R. MacCartney and T. S. Rappaport, "73 ghz millimeter wave propagation measurements for outdoor urban mobile and backhaul communications in new york city," in *2014 IEEE International Conference on Communications (ICC)*, 2014, pp. 4862–4867.
- [5] M. K. Samimi, T. S. Rappaport, and G. R. MacCartney, "Probabilistic omnidirectional path loss models for millimeter-wave outdoor communications," *IEEE Wireless Communications Letters*, vol. 4, no. 4, pp. 357–360, 2015.
- [6] X. Zhao, S. Li, Q. Wang, M. Wang, S. Sun, and W. Hong, "Channel measurements, modeling, simulation and validation at 32 ghz in outdoor microcells for 5g radio systems," *IEEE Access*, vol. 5, pp. 1062–1072, 2017.
- [7] Y. Xing and T. S. Rappaport, "Millimeter wave and terahertz urban microcell propagation measurements and models," *IEEE Communications Letters*, vol. 25, no. 12, pp. 3755–3759, 2021.
- [8] B. De Beelde, D. Plets, C. Desset, E. Tanghe, A. Bourdoux, and W. Joseph, "Material characterization and radio channel modeling at d-band frequencies," *IEEE Access*, vol. 9, pp. 153 528–153 539, 2021.
- [9] B. De Beelde, E. Tanghe, D. Plets, and W. Joseph, "Outdoor line-of-sight path loss modeling at 140 ghz," in *2022 16th European Conference on Antennas and Propagation (EuCAP)*, 2022, pp. 1–4.
- [10] T. Schneider, A. Wiatrek, S. Preussler, M. Grigat, and R.-P. Braun, "Link budget analysis for terahertz fixed wireless links," *IEEE Transactions on Terahertz Science and Technology*, vol. 2, no. 2, pp. 250–256, 2012.
- [11] A. E. Drougas, A. D. Panagopoulos, and P. G. Cottis, "Packet error statistics of los broadband fixed wireless access channels," *IEEE Transactions on Communications*, vol. 57, no. 1, pp. 22–25, 2009.
- [12] Z. A. Shamsan, "Rainfall and diffraction modeling for millimeter-wave wireless fixed systems," *IEEE Access*, vol. 8, pp. 212 961–212 978, 2020.
- [13] M. A. Weissberger, "An initial critical summary of models for predicting the attenuation of radio waves by trees," Final Report Electromagnetic Compatibility Analysis Center, Jul. 1982.
- [14] I. R. C. Committee, *Recommendations and Reports of the CCIR, 1986: Propagation in non-ionized media*, ser. Recommendations and Reports of the CCIR, 1986. International Telecommunication Union, 1986.
- [15] A. Lagrone, "Propagation of vhf and uhf electromagnetic waves over a grove of trees in full leaf," *IEEE Transactions on Antennas and Propagation*, vol. 25, no. 6, pp. 866–869, 1977.
- [16] G. Dooren, van, H. Govaerts, and M. Herben, *COST 235: Radiowave propagation effects on next-generation fixed-services terrestrial telecommunications systems*. Technische Universiteit Eindhoven, 1997.
- [17] M. Al-Nuaimi and R. Stephens, "Measurements and prediction model optimisation for signal attenuation in vegetation media at centimetre wave frequencies," *IEE Proceedings - Microwaves, Antennas and Propagation*, vol. 145, pp. 201–206(5), June 1998.
- [18] "Attenuation in vegetation, recommendation itu-r p.833-10," International Telecommunication Union, Tech. Rep., 2021.
- [19] M. H. C. Dias and M. S. de Assis, "An empirical model for propagation loss through tropical woodland in urban areas at uhf," *IEEE Transactions on Antennas and Propagation*, vol. 59, no. 1, pp. 333–335, 2011.
- [20] A. Seville and K. Craig, "Semi-empirical model for millimetre-wave vegetation attenuation rates," *Electronics Letters*, vol. 31, pp. 1507–1508(1), August 1995.
- [21] A. Seville, "Vegetation attenuation: modelling and measurements at millimetric frequencies," in *Tenth International Conference on Antennas and Propagation (Conf. Publ. No. 436)*, vol. 2, 1997, pp. 5–8 vol.2.

- [22] N. Savage, D. Ndzi, A. Seville, E. Vilar, and J. Austin, "Radio wave propagation through vegetation: Factors influencing signal attenuation," *Radio Science*, vol. 38, no. 5, 2003.
- [23] A. N. Romanov and P. N. Ulanov, "Seasonal differences in dielectric properties of dwarf woody tundra vegetation in a microwave range," *IEEE Transactions on Geoscience and Remote Sensing*, vol. 57, no. 6, pp. 3119–3125, 2019.
- [24] F. Schwing, E. Violette, and R. Espeland, "Millimeter-wave propagation in vegetation: experiments and theory," *IEEE Transactions on Geoscience and Remote Sensing*, vol. 26, no. 3, pp. 355–367, 1988.
- [25] P. Horak, M. Kvicera, and P. Pechac, "Frequency dependence of attenuation due to vegetation for satellite services," *IEEE Antennas and Wireless Propagation Letters*, vol. 9, pp. 142–144, 2010.
- [26] J. A. R. Azevedo and F. E. S. Santos, "An empirical propagation model for forest environments at tree trunk level," *IEEE Transactions on Antennas and Propagation*, vol. 59, no. 6, pp. 2357–2367, 2011.
- [27] J. Hejlselbaek, J. Ødum Nielsen, W. Fan, and G. F. Pedersen, "Empirical study of near ground propagation in forest terrain for internet-of-things type device-to-device communication," *IEEE Access*, vol. 6, pp. 54 052–54 063, 2018.
- [28] D. Liao and K. Sarabandi, "Modeling and simulation of near-earth propagation in presence of a truncated vegetation layer," *IEEE Transactions on Antennas and Propagation*, vol. 55, no. 3, pp. 949–957, 2007.
- [29] L. DaHan and K. Sarabandi, "Near-earth wave propagation characteristics of electric dipole in presence of vegetation or snow layer," *IEEE Transactions on Antennas and Propagation*, vol. 53, no. 11, pp. 3747–3756, 2005.
- [30] S. Perras and L. Bouchard, "Fading characteristics of rf signals due to foliage in frequency bands from 2 to 60 ghz," in *The 5th International Symposium on Wireless Personal Multimedia Communications*, vol. 1, 2002, pp. 267–271 vol.1.
- [31] Y. Zhang, C. R. Anderson, N. Michelusi, D. J. Love, K. R. Baker, and J. V. Krogmeier, "Propagation modeling through foliage in a coniferous forest at 28 ghz," *IEEE Wireless Communications Letters*, vol. 8, no. 3, pp. 901–904, 2019.
- [32] Y. Lv, X. Yin, C. Zhang, and H. Wang, "Measurement-based characterization of 39 ghz millimeter-wave dual-polarized channel under foliage loss impact," *IEEE Access*, vol. 7, pp. 151 558–151 568, 2019.
- [33] P. Zhang, B. Yang, C. Yi, H. Wang, and X. You, "Measurement-based 5g millimeter-wave propagation characterization in vegetated suburban macrocell environments," *IEEE Transactions on Antennas and Propagation*, vol. 68, no. 7, pp. 5556–5567, 2020.
- [34] J. Ko, S. Hur, Y.-S. Noh, K. Whang, J. Park, D.-J. Park, and D.-H. Cho, "Measurements and analysis of radio propagation at 28 ghz in vegetated areas of typical residential environments," *IEEE Transactions on Antennas and Propagation*, vol. 68, no. 5, pp. 4149–4154, 2020.
- [35] N. C. Rogers, A. Seville, J. Richter, D. L. Ndzi, N. Savage, R. F. S. Caldeirinha, A. K. Shukla, M. O. Al-Nuaimi, K. H. Craig, E. Vilar, and J. Austin, "A generic model of 1-60 ghz radio propagation through vegetation-final report," Radiocommunications Agency, Tech. Rep., 2002.
- [36] N. R. Leonor, R. F. S. Caldeirinha, T. R. Fernandes, J. Richter, and M. Al-Nuaimi, "A discrete ret model for millimeter-wave propagation through vegetation," *IEEE Transactions on Antennas and Propagation*, vol. 66, no. 4, pp. 1985–1998, 2018.
- [37] N. R. Leonor, M. G. Sánchez, T. R. Fernandes, and R. F. S. Caldeirinha, "A 2d ray-tracing based model for wave propagation through forests at micro-and millimeter wave frequencies," *IEEE Access*, vol. 6, pp. 32 097–32 108, 2018.
- [38] N. R. Leonor, T. R. Fernandes, M. García Sánchez, and R. F. S. Caldeirinha, "A 3-d model for millimeter-wave propagation through vegetation media using ray-tracing," *IEEE Transactions on Antennas and Propagation*, vol. 67, no. 6, pp. 4313–4318, 2019.
- [39] P. Horak and P. Pechac, "Excess loss for high elevation angle links shadowed by a single tree: Measurements and modeling," *IEEE Transactions on Antennas and Propagation*, vol. 60, no. 7, pp. 3541–3545, 2012.
- [40] S. Liang, X. Li, and J. Wang, "Chapter 13 - fractional vegetation cover," in *Advanced Remote Sensing*. Boston: Academic Press, 2012, pp. 415–438.
- [41] T. M. Saitoh, S. Nagai, H. M. Noda, H. Muraoka, and K. N. Nasahara, "Examination of the extinction coefficient in the beer-lambert law for an accurate estimation of the forest canopy leaf area index," *Forest Science and Technology*, vol. 8, no. 2, pp. 67–76, 2012.
- [42] C.-W. Tan, P.-P. Zhang, X.-X. Zhou, Z.-X. Wang, Z.-Q. Xu, W. Mao, W.-X. Li, Z.-Y. Huo, W.-S. Guo, and F. Yun, "Quantitative monitoring of leaf area index in wheat of different plant types by integrating ndvi and beer-lambert law," *Scientific Reports*, vol. 10, no. 1, p. 929, 2020.
- [43] H. Fang, F. Baret, S. Plummer, and G. Schaepman-Strub, "An overview of global leaf area index (lai): Methods, products, validation, and applications," *Reviews of Geophysics*, vol. 57, no. 3, pp. 739–799, September 2019.
- [44] S. A. Sytnyk and P. I. Lakyda, "Leaf area index of black locust stands in northern steppe of ukraine," *Forestry and Forest Melioration*, no. 131, p. 143–149, Feb. 2018.
- [45] N. J. J. Bréda, "Ground-based measurements of leaf area index: a review of methods, instruments and current controversies," *Journal of Experimental Botany*, vol. 54, no. 392, pp. 2403–2417, 11 2003.
- [46] I. C. Meier and C. Leuschner, "Leaf size and leaf area index in fagus sylvatica forests: Competing effects of precipitation, temperature, and nitrogen availability," *Ecosystems*, vol. 11, no. 5, pp. 655–669, 2008.
- [47] E. Dufrene and N. Bréda, "Estimation of deciduous forest leaf area index using direct and indirect methods," *Oecologia*, vol. 104, no. 2, pp. 156–162, 1995.
- [48] 3GPP, "Study on channel model for frequencies from 0.5 to 100 ghz," *Technical report (TR) 38.901, 3rd Generation Partnership Project (3GPP)*, 2017.
- [49] S. Gurdebeke, D. De Bakker, N. Vanlanduyt, and J. Maelfait, "Plans for a large regional forest in eastern flanders (belgium): assessment of spider diversity and community structure in the current forest remnants," *BIODIVERSITY AND CONSERVATION*, vol. 12, no. 9, pp. 1883–1900, SEP 2003.
- [50] K. De Pauw, P. Sanczuk, C. Meeussen, L. Depauw, E. De Lombaerde, S. Govaert, T. Vanneste, J. Brunet, S. A. O. Cousins, C. Gasperini, P.-O. Hedwall, G. Iacopetti, J. Lenoir, J. Plue, F. Selvi, F. Spicher, J. Uria-Diez, K. Verheyen, P. Vangansbeke, and P. De Frenne, "Forest understorey communities respond strongly to light in interaction with forest structure, but not to microclimate warming," *New Phytologist*, vol. 233, no. 1, pp. 219–235, 2022.
- [51] G. Frazer, C. Canham, , and K. Lertzman, *Gap Light Analyzer (GLA): Imaging software to extract canopy structure and gap light transmission indices from true-colour fisheye photographs*. Simon Fraser University, Burnaby, British Columbia, and the Institute of Ecosystem Studies, Millbrook, New York, 1999.
- [52] B. De Beelde, D. Plets, E. Tanghe, C. Li, and W. Joseph, "V-band rain attenuation measurement setup," in *2022 3rd URSI AT-AP-RASC, Gran Canaria, 29 May – 3 June 2022*, 2022, pp. 1–4.
- [53] R. F. Caldeirinha, T. R. Fernandes, J. Richter, and M. O. Al-Nuaimi, "Simplified ret model derived from path loss and directional spectrum measurements in vegetation media at 11.2 and 20 ghz," *IET Microwaves, Antennas & Propagation*, vol. 11, no. 1, pp. 136–143, 2017.
- [54] J. Scurlock, "Worldwide historical estimates of leaf area index, 1932-2000," U.S. Department of Energy, Office of Scientific and Technical Information, Tech. Rep., 2 2002.
- [55] A. IIO and A. ITO, "A global database of field-observed leaf area index in woody plant species, 1932-2011," 2014.
- [56] J. Černý, P. Haninec, and R. Pokorný, "Leaf area index estimated by direct, semi-direct, and indirect methods in european beech and sycamore maple stands," *Journal of Forestry Research*, vol. 31, no. 3, pp. 827–836, 2020.
- [57] P. Köhler and A. Huth, "Towards ground-truthing of spaceborne estimates of above-ground life biomass and leaf area index in tropical rain forests," *Biogeosciences*, vol. 7, no. 8, pp. 2531–2543, 2010.
- [58] D. Zhang, J. Liu, W. Ni, G. Sun, Z. Zhang, Q. Liu, and Q. Wang, "Estimation of forest leaf area index using height and canopy cover information extracted from unmanned aerial vehicle stereo imagery," *IEEE Journal of Selected Topics in Applied Earth Observations and Remote Sensing*, vol. 12, no. 2, pp. 471–481, 2019.
- [59] S. Munier, D. Carrer, C. Planque, F. Camacho, C. Albergel, and J.-C. Calvet, "Satellite leaf area index: Global scale analysis of the tendencies per vegetation type over the last 17 years," *Remote Sensing*, vol. 10, no. 3, 2018.





(a) Environment 1



(b) Environment 2



(c) Environment 3



(d) Environment 4



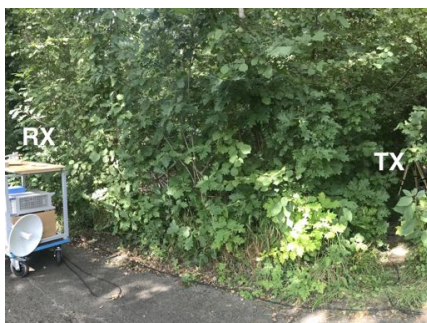
(e) Environment 5



(f) Environment 6



(g) Environment 7



(h) Environment 8



(i) Environment 9



(j) Environment 10



(k) Environment 11



(l) Environment 12

Figure 8. Measurement environments.



## SUPPLEMENTARY MATERIAL

### A. Plant area index estimation

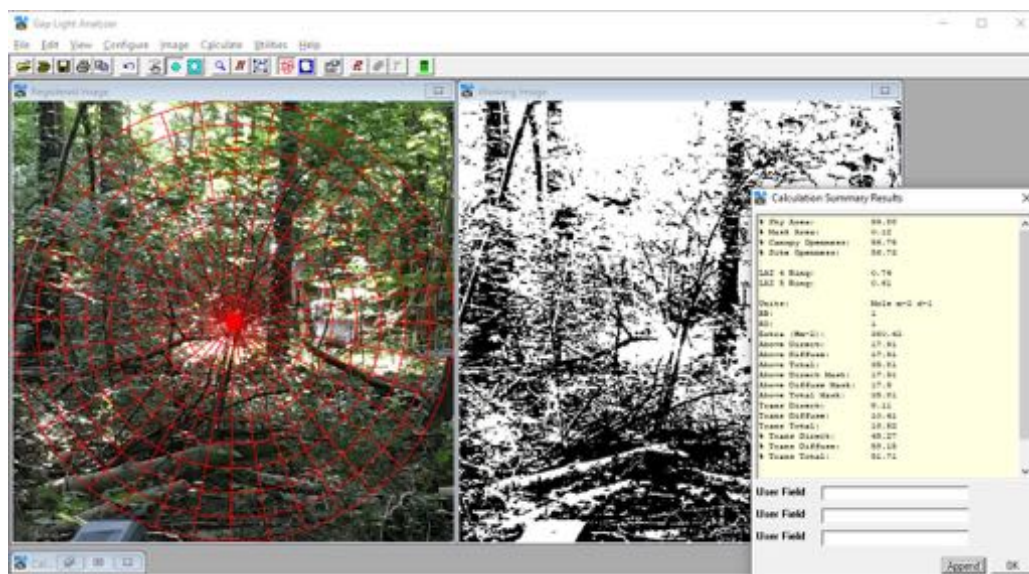
For each measurement, i.e., each measurement environment and vegetation depth, we perform a plant area index (PAI) estimation using three different methodologies.

- 1) Literature review
- 2) On-site estimation of vegetation density
- 3) A picture that is taken during the measurements, and analyzed using the Gap Light Analyzer (GLA) tool [51]

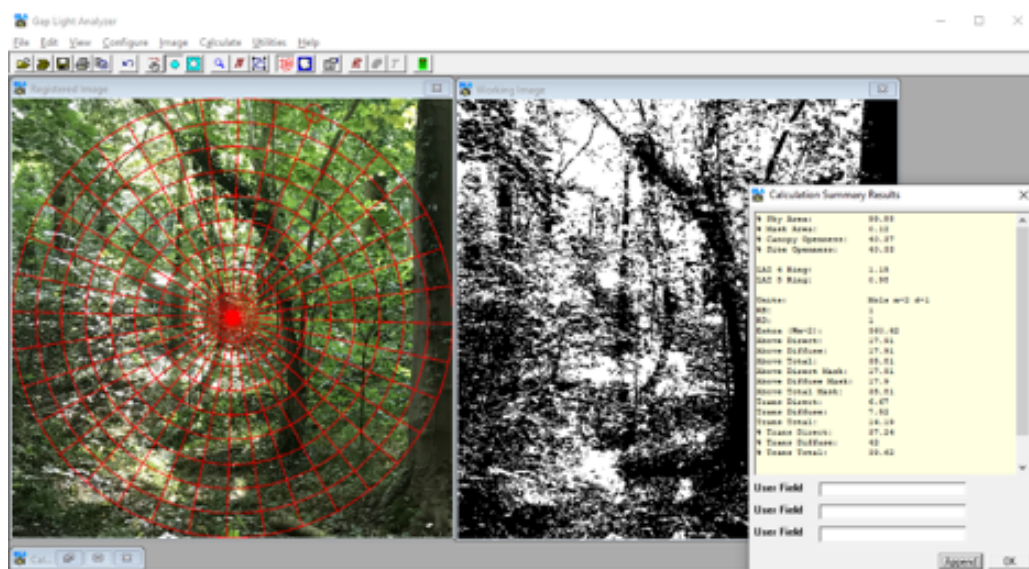
Instructions for using the GLA tool:

- Register an image, draw a circle around the vegetation that is present at breast height
- Setup configuration: enter GPS data, solar constant of 1361, cloudy sky transmission coefficient, and set growing season start date to March and end date to October
- Select the blue color plane and use overlay sky region grid
- Set the threshold of the image so that the plants are colored black, and open space is colored white
- Run the calculation

An example for the GLA analysis for two distances of measurement environment 6 is provided in Fig. 9.



(a) Distance 18.3



(b) Distance 27.6 m

Figure 9. Gap Light Analyzer for two measurements from environment 6.

### B. Reference measurements

The measurement setup for the Line-of-Sight reference measurements is shown in Fig. 10 for an antenna separation of 5 m. Figure 11 shows the measured PL and free space PL for the different distances, as well as the statistics of the error between measured PL and free space PL as a function of frequency.

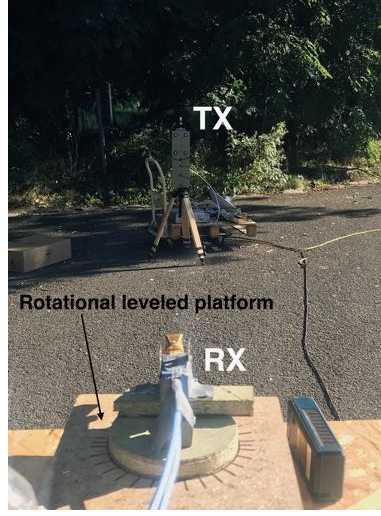
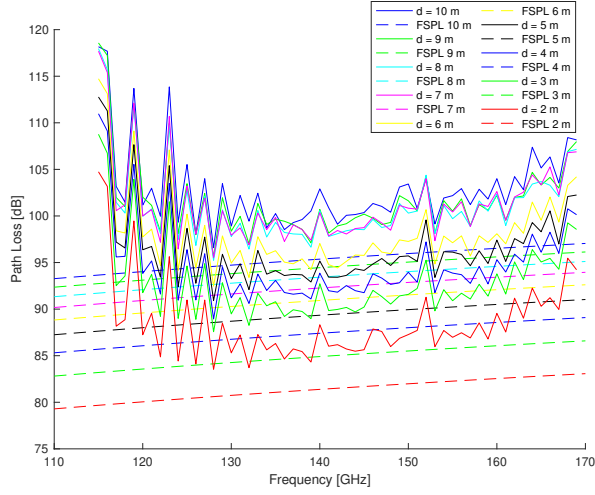
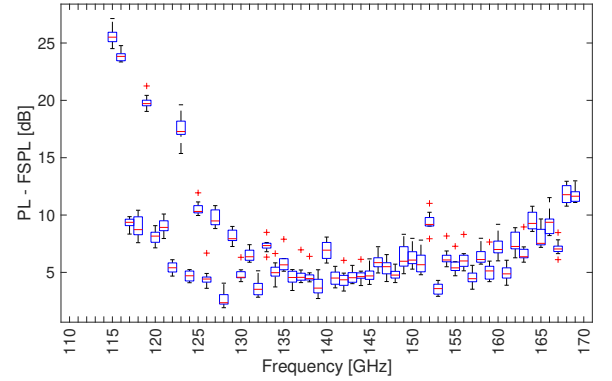


Figure 10. Outdoor reference measurement setup for Line-of-Sight distance 5 m.



(a) Measured PL and free space PL as a function of frequency for distances ranging from 2 to 10 m



(b) Five-number summary of error between measured PL and FSPL

Figure 11. Outdoor reference measurement results.